Raman scattering study and lattice-dynamics investigation of the $NaMnF_3$ perovskite

Ph. Daniel, M. Rousseau, and A. Desert
Laboratoire de Physique de l'Etat Condensé, URA CNRS 807, Université du Maine, Avenue Olivier Messiaen, 72017 Le Mans, France

A. Ratuszna
Institute of Physics, University of Silesia 4, ul. Uniwersytecka, 40007 Katowice, Poland

F. Ganot
Laboratoire des Propriétés Mécaniques et Thermodynamiques des Matériaux, CNRS UPR 9001, Université Paris Nord, Avenue J.B. Clément, 93430 Villetaneuse, France

(Received 31 October 1994)

In the framework of the study of structural phase transitions in fluoroperovskites AMF_3, sodium manganese fluoride $NaMnF_3$ is especially interesting because it is a rare distorted perovskite that can be obtained easily as a monodomain sample in an orthorhombic low-temperature phase. X-ray experiments were performed to confirm this quasimonodomain character. Raman spectra of $NaMnF_3$ were recorded and interpreted between 40 and 573 K. From group-theory analysis it was shown that the orthorhombic-cubic high-temperature phase transition which occurs in $NaMnF_3$ can be imputed to the condensation of vibrational modes located at the Γ, R, M, and X points of the first cubic Brillouin zone. Assuming that the Raman modes which are not responsible for the transition are temperature independent and with help from compatibility diagrams, frequencies of high-symmetry zone boundary modes in the high-temperature phase (cubic symmetry) were deduced only from experimental data obtained in the orthorhombic phase. Consequently these data were used to adjust the parameters of a rigid-ion model in the ideal cubic phase. The calculated phonon spectrum and the phonon density of states were deduced. The calculated cubic elastic constants C_{11}, C_{12}, C_{44} are consistent with the elastic constants measured by Brillouin scattering in the quasicubic approximation. Moreover, the reported Raman study provides evidence for the occurrence of a two-magnon scattering due to antiferromagnetic character below $T_N = 60$ K with persistence of a broad line above the Néel temperature.

INTRODUCTION

In the past few years, many studies have been performed on AMF_3 fluoroperovskites, with the goal of understanding the mechanisms of the structural phase transitions (SPT) occurring in these compounds.[1–8]

Many AMF_3 compounds crystallize in the ideal cubic perovskite structure in their highest temperature phase. When lowering temperature this structure is frequently modified by the tilting of MF_6 octahedra. An exhaustive description and classification of octahedral tilting in perovskites has been done by Glazer.[9] According to Kassan-Ogly and Naish,[10] the highest-temperature phase is not cubic but pseudocubic and the lowest-temperature phase called "ground state" should correspond to static tilts around the three pseudocubic axes. This ground state of orthorhombic symmetry was predicted by Flocken *et al.*[1] from calculations based upon *ab initio* interionic potentials obtained by the Gordon-Kim approach. Between the cubic phase (no tilt) and the ground state (three tilts) various intermediate states associated to one or two tilts are predicted by Glazer.[9] According to this author, the octahedra rotations around the O_x cubic axis will be noted a^0, a^+, or a^-, where the superscripts 0, +, or − indicate whether successive octahedra along the a axis have no tilt, the same tilt, or opposite tilt about that axis.

Among these compounds, $NaMnF_3$ appears to be an original and interesting case because the lack of any intermediate phase between the cubic phase and the orthorhombic ground state allows for the growth of monodomain samples of orthorhombic $NaMnF_3$. This monodomain character will allow us to assign unambiguously the Raman spectra of this compound; in fact, in other fluoroperovskites, because of the domains structure, many unsuccessful attempts were performed in Raman field. Then, in the future, on the basis of the suggested interpretation of Raman results presented here for $NaMnF_3$, it would enable the attribution of Raman lines in other isostructural perovskites.

In this paper after a short review of the structural data, we report Raman scattering results recorded between 40 and 573 K in $NaMnF_3$. The assignment of Raman lines is proposed from a group-theory analysis of the orthorhombic phase. From these experimental data, short-range force constants are estimated and the whole phonon spectrum of the high-temperature cubic phase is calculated in the framework of a rigid ion model.

EXPERIMENTAL DETAILS

Two $NaMnF_3$ samples were prepared by a modified Bridgmann-Stockbarger crystal growth method, either in a horizontal furnace[11] or in a vertical furnace.[12] In all cases crystals were obtained from a stoichiometric mix-

0163-1829/95/51(18)/12337(10)/$06.00

ture of purified materials $NaF+MnF_2$, introduced in a graphite crucible and melted at about 820 °C under inert atmosphere. An adapted temperature protocol with a cooling rate of 1 °C/h down to 600 °C was used. Blocks of pink color crystals with a good optical quality could be extract from the crucible.

A first sample was cut and oriented by the x-ray Laüe method along *pseudocubic* axes that are in the orthorhombic cell, the three directions $[101]_o$, $[010]_o$, and $[10\bar{1}]_o$, respectively labeled a_c, b_c, and c_c (o and c subscripts indicate, respectively, orthorhombic and cubic cells). The second sample was cut along *orthorhombic* axes labeled a_o, b_o, and c_o.

From x-ray diffraction, it was observed that the $[001]_o$ face consisted of 99% of a_o domains and 1% of disoriented c_o domains without existence of b_o domains. Likewise the $[001]_o$ face is constituted of 93% of c_o domains and 7% of a_o domains. Observation of the $[010]_o$ face (natural split face) evidenced the existence of only b_o domains. Samples used in Raman scattering measurements could be thus considered as quasimonodomain crystals. This monodomain aptitude is very rare for fluoroperovskites [$KCaF_3$ (Ref. 13), $KMnF_3$ (Ref. 2)] which undergo cubic-tetragonal-orthorhombic SPT, and then are generally constituted of a disoriented mixing of the three domains a_o, b_o, c_o. This singular property of $NaMnF_3$ is probably due to the nonexistence of the intermediate tetragonal phase; indeed in this compound only one SPT occurs between cubic and orthorhombic symmetry.[14]

Raman spectra were recorded with a Dilor Z24 spectrometer triple monochromator, coupled with a Coherent 90-3 laser beam. The incident selected wavelengths were the 514.5- and 488-nm lines. Comparison between Raman spectra recorded in the same conditions, but with these two different wavelengths, evidenced that no contamination has been observed by fluorescence lines. An incident power of 500 mW was used. Low-temperature measurements were performed up to 40 K with help of a Leybold cryogenerator and high-temperature experiments could be realized under microscope with a Chaix-Meca heating cell. According to experimental configuration high-temperature measurements were done on a microscopic sample (1–2 mm^3), only with the goal to study the temperature evolution of Raman modes and determine which modes are responsible for the transition. Intense Raman lines could be followed up to 573 K; above this temperature the crystals were quickly damaged under laser beam.

The elastic constants were deduced from Brillouin scattering measurements using a five-pass piezoelectrically driven Fabry-Pérot interferometer. The sample was illuminated by the 514.5-nm line of a single-mode argon laser with a power around 300 mW. The average refractive index of the crystal was determined for this wavelength using a Pülfrich refractometer. For light analysis, 180° or 90° scattering geometries were chosen according to well-defined selection rules. In a pseudocubic approximation, only three independent elastic constants exist, namely, C_{11}, C_{12}, and C_{44}, which are straightforwardly associated to acoustic phonon wave vectors parallel to high-symmetry crystalline axes. However, one has to take into account the orthorhombic distortion, which induces some variations in the measurements along equivalent directions of the pseudocubic structure. Concerning C_{11} and C_{44}, these experimentally measured variations do not exceed 4%. The determinations of C_{12} lie in a larger range: they arise from indirect calculations using the measurements of linear combinations of the other constants involving complicated mixing of the nonvanishing transverse orthorhombic constants and more dramatically of the longitudinal orthorhombic C_{11} and C_{33}, which exhibit a difference of about 20%. Notice, on the other hand, that the orthorhombic distortion does not induce noticeable birefringence effects: within the Brillouin experimental uncertainty, we estimate them to be less than 0.05%. Finally no splitting or measurable broadening of the Brillouin lines could be observed, confirming the above-mentioned quasimonodomain character of the crystals.

The x-ray measurements were performed using a double crystal x-ray diffractometer. The direct beam was collimating by a set of two slits and the x-ray beam scattered by a crystal was analyzed with a bent pyrolitic graphite in front of which were set two narrow slits. The experiments were performed in a reflection geometry at room temperature from the three orthorhombic directions.

GROUP-THEORY ANALYSIS

The structure of $NaMnF_3$ at room temperature is orthorhombic[15] with *Pnma* space group [$a_o=5.751(4)$ Å, $b_o=8.008(6)$ Å, $c_o=5.548(4)$ Å], resulting from a distortion of the ideal cubic perovskite symmetry. This deformation is caused by a tilting of the octahedra according to the sequence $a^-b^+a^-$ (Glazer's labeling[9]) but also by a deformation of the octahedra and displacement of the Na^+ cation from their ideal position along $[101]_c$. Figure 1 compares the connection between MnF_6 octahedra in the aristotype structure (a) and the distorted one (b). As previously indicated, the tetragonal phase does not exist, however a SPT was detected at 965 K (Ref. 14) between

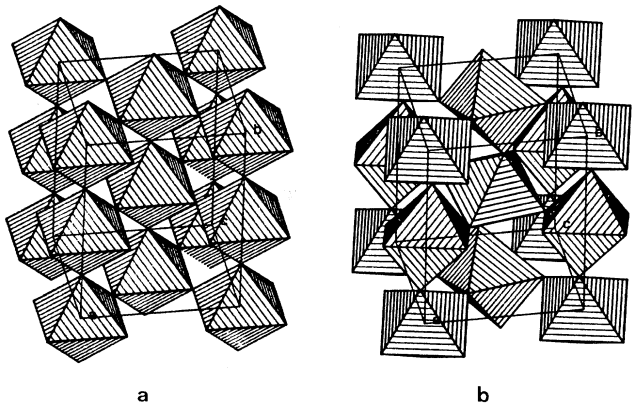

FIG. 1. Ideal arrangement of MnF_6 octahedra in the cubic symmetry (a) compared to the corresponding arrangement in the orthorhombic distorted phase (b).

TABLE I. Irreducible representations of the D_{2h} point group associated with the motion of the three different atoms in $NaMnF_3$. The first four lines give results according to the atom positions deduced from structural data (Ref. 9). Γ_{optic} summarizes all optic vibrational modes and Γ_{Raman} correspond to Raman active g modes.

$$\Gamma_{Na}=2A_g\oplus B_{1g}\oplus 2B_{2g}\oplus B_{3g}\oplus A_u\oplus 2B_{1u}\oplus B_{2u}\oplus 2B_{3u}$$
$$\Gamma_{Mn}=3A_u\oplus 3B_{1u}\oplus 3B_{2u}\oplus 3B_{3u}$$
$$\Gamma_{F1}=3A_g\oplus 3B_{1g}\oplus 3B_{2g}\oplus 3B_{3g}\oplus 3A_u\oplus 3B_{1u}\oplus 3B_{2u}\oplus 3B_{3u}$$
$$\Gamma_{F2}=2A_g\oplus B_{1g}\oplus 2B_{2g}\oplus B_{3g}\oplus A_u\oplus 2B_{1u}\oplus B_{2u}\oplus 2B_{3u}$$
$$\Gamma_{optic}=7A_g\oplus 5B_{1g}\oplus 7B_{2g}\oplus 5B_{3g}\oplus 8A_u\oplus 9B_{1u}\oplus 7B_{2u}\oplus 9B_{3u}$$
$$\Gamma_{Raman}=7A_g\oplus 5B_{1g}\oplus 7B_{2g}\oplus 5B_{3g}$$

the orthorhombic phase ($a^-b^+a^-$) and the ideal cubic phase ($a^0a^0a^0$).

In order to correctly interpret the Raman spectra in the orthorhombic phase, a decomposition of the eigenmodes of vibration according to the method previously described by Rousseau, Baumann, and Porto[16] was performed at the center of the orthorhombic Brillouin zone. As shown in Table I, the Raman active modes could be deduced from these calculations, and 24 Raman lines are expected, respectively: $7A_g$, $5B_{1g}$, $7B_{2g}$ and $5B_{3g}$. These modes can be distinguished in the spectra according to the selection rules of Raman scattering (Raman tensors); Table II summarizes the predicted Raman lines according to configurations and selection rules.

The orthorhombic symmetry of sodium manganese fluoride $NaMnF_3$ constitutes a weakly distorted phase from the ideal cubic type, moreover lattice-dynamics calculations in the ideal cubic phase are easier and need less parameters than in the orthorhombic one. However, in order to perform such calculations in the cubic phase with the help of Raman results obtained only in the room-temperature phase, it is necessary to establish the link between the two structures from a group-theory point of view.

The correspondence between cubic and orthorhombic cells in the direct lattice is given by

TABLE II. Selection rules for Raman scattering active modes in the $NaMnF_3$ orthorhombic phase.

Raman tensors: $O_z\|C_{2z}$ $O_x\|\sigma_y$

$$A_g=\begin{vmatrix} a & & \\ & b & \\ & & c \end{vmatrix} \quad B_{1g}\begin{vmatrix} & d & \\ d & & \\ & & \end{vmatrix} \quad B_{2g}\begin{vmatrix} & & e \\ & & \\ e & & \end{vmatrix} \quad B_{3g}\begin{vmatrix} & & \\ & & f \\ & f & \end{vmatrix}$$

Expected Raman lines according Porto's labeling:

a_o,b_o,c_o indicate orthorhombic axes and a_c,b_c,c_c are used for cubic axes.

$c_o(a_oa_o)b_o$:$7A_g$ $c_o(a_oc_o)b_o$:$7B_{2g}$ $c_c(a_ca_c)b_c$:$7A_g\oplus 7B_{2g}$ $c_c(a_cc_c)b_c$:$7A_g$

$b_o(a_oa_o)c_o$:$7A_g$ $b_o(a_ob_o)c_o$:$5B_{1g}$ $b_c(a_ca_c)c_c$:$7A_g\oplus 7B_{2g}$ $b_c(a_cb_c)c_c$:$5B_{1g}\oplus 5B_{3g}$

$a_o(b_ob_o)c_o$:$7A_g$ $a_o(b_oa_o)c_o$:$5B_{1g}$ $a_c(b_cb_c)c_c$:$7A_g$ $a_c(b_ca_c)c_c$:$5B_{1g}\oplus 5B_{3g}$

$c_o(b_ob_o)a_o$:$7A_g$ $c_o(b_oc_o)a_o$:$5B_{3g}$ $c_c(b_cb_c)a_c$:$7A_g$ $c_c(b_cc_c)a_c$:$5B_{1g}\oplus 5B_{3g}$

$a_o(c_oc_o)b_o$:$7A_g$ $a_o(c_oc_o)b_o$:$7B_{2g}$ $a_c(c_cc_c)b_c$:$7A_g\oplus 7B_{2g}$ $a_c(c_cc_c)b_c$:$5B_{1g}\oplus 5B_{3g}$

$b_o(c_oc_o)a_o$:$7A_g$ $b_o(c_ob_o)a_o$:$5B_{3g}$ $b_c(c_cc_c)a_c$:$7A_g\oplus 7B_{2g}$ $b_c(c_cb_c)a_c$:$5B_{1g}\oplus 5B_{3g}$

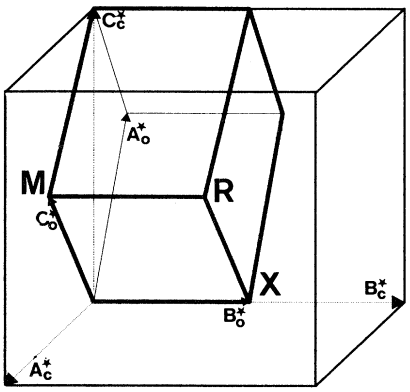

FIG. 2. Correspondence between orthorhombic and cubic Brillouin zones. A_c^*, B_c^*, C_c^* indicate vectors of the reciprocal cubic lattice. A_o^*, B_o^*, C_o^* indicate vectors of the reciprocal orthorhombic lattice.

$$\mathbf{a}_o=\mathbf{a}_c-\mathbf{c}_c,\quad \mathbf{b}_o=2\mathbf{b}_c,\quad \mathbf{c}_o=\mathbf{a}_c+\mathbf{c}_c\ ,$$

$$\mathbf{a}_c=\tfrac{1}{2}(\mathbf{a}_o+\mathbf{c}_o),\quad \mathbf{b}_c=\tfrac{1}{2}\mathbf{b}_o,\quad \mathbf{c}_c=-\tfrac{1}{2}(\mathbf{a}_o-\mathbf{c}_o)\ ,$$

where $\mathbf{a}_o,\mathbf{b}_o,\mathbf{c}_o$ are the orthorhombic cell vectors and $\mathbf{a}_c,\mathbf{b}_c,\mathbf{c}_c$ the cubic cell vectors in the direct lattice. In the reciprocal lattice these relations become

$$\mathbf{A}_o^*=\tfrac{1}{2}(\mathbf{A}_c^*-\mathbf{C}_c^*),\quad \mathbf{B}_o^*=\tfrac{1}{2}\mathbf{B}_c^*,\quad \mathbf{C}_o^*=\tfrac{1}{2}(\mathbf{A}_c^*+\mathbf{C}_c^*)\ ,$$

$$\mathbf{A}_c^*=\mathbf{A}_o^*+\mathbf{C}_o^*,\quad \mathbf{B}_c^*=2\mathbf{B}_o^*,\quad \mathbf{C}_c^*=-\mathbf{A}_o^*+\mathbf{C}_o^*\ ,$$

where $\mathbf{A}_o^*,\mathbf{B}_o^*,\mathbf{C}_o^*$ ($\mathbf{A}_c^*,\mathbf{B}_c^*,\mathbf{C}_c^*$) are the reciprocal vectors in the orthorhombic reciprocal cell (reciprocal cubic cell). Then using these last relations, it is shown that vibrational modes located at the $\Gamma_o(0,0,0)$ point of the orthorhombic Brillouin zone come from modes located at the $\Gamma_c(0,0,0)$, $R_c(1/2,1/2,1/2)$, $M_c(1/2,0,1/2)$, and $X_c(0,1/2,0)$ points of the first cubic Brillouin zone where X_c, M_c, R_c are zone-boundary points:

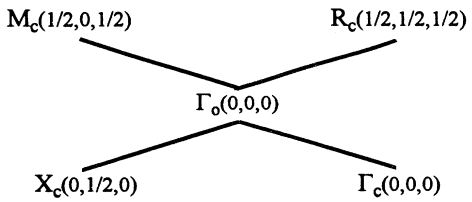

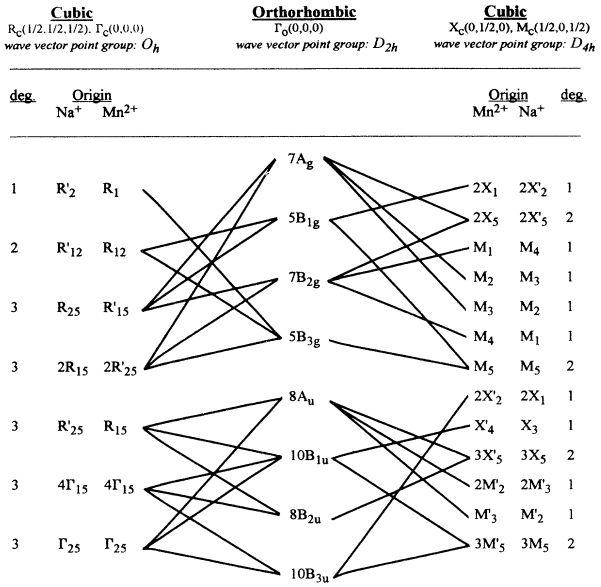

FIG. 3. Compatibility diagrams of the symmetries between the orthorhombic Γ_o point and the Γ_c, M_c, X_c, R_c cubic points. Wave-vector point groups are in italics. Cubic vibration modes are labeled according to Koster notation. Correspondence between modes, according to origin calculation, is indicated. "deg" indicates degeneracy of modes.

Figure 2 illustrates correspondence between cubic and orthorhombic Brillouin zone. Decomposition on the reducible mechanical representation at the Γ_c, M_c, R_c, X_c points of the first cubic Brillouin zone was then performed for the $NaMnF_3$ cubic phase. The origin of the cubic cell was chosen on the Mn^{2+} ion for all calculations. Table III summarizes the results of these decompositions. Thus compatibility relations between irreducible representations at the Γ_o point of the orthorhombic Brillouin zone and the Γ_c, M_c, R_c, X_c points of the cubic Brillouin zone were established. Figure 3 illustrates these relations as schematic diagrams (on this diagram a correspondence between labeling of eigenmodes according to origin choice is given for comparison with previous papers).

RAMAN SCATTERING STUDY

Raman scattering experiments were performed between 40 and 573 K using two samples oriented, as previ-

TABLE III. Decomposition of the mechanical representation in the $NaMnF_3$ cubic phase at the $\Gamma_c(0,0,0)$, $M_c(1/2,0,1/2)$, $X_c(0,1/2,0)$, $R_c(1/2,1/2,1/2)$ points of the first cubic Brillouin zone. Origin on Mn^{2+} ion; Koster labeling.

$$\Gamma_{\Gamma_c(0,0,0)}=4\Gamma_{15}\oplus\Gamma_{25}$$
$$\Gamma_{M_c(1/2,0,1/2)}=M_1\oplus M_2\oplus M_3\oplus M_4\oplus M_5\oplus 2M_2'\oplus M_3'\oplus 3M_5'$$
$$\Gamma_{X_c(0,1/2,0)}=2X_1\oplus 2X_5\oplus 2X_2'\oplus X_4'\oplus 3X_5'$$
$$\Gamma_{R_c(1/2,1/2,1/2)}=R_1\oplus R_{12}\oplus R_{15}'\oplus 2R_{25}'\oplus R_{15}$$

TABLE IV. Assignment of $NaMnF_3$ Raman lines at 40 and 300 K.

Raman mode	Predicted	Observed	T (K)	Frequencies (cm^{-1})
A_g	7	7	40	88-143-183-212-250-270-319
			300	96-140-165-202-236-264-308
B_{1g}	5	4	40	160-182-312-426
			300	159-?-296-426
B_{2g}	7	5	40	140-155-201-226-293
			300	135-?-184-226-287
B_{3g}	5	2	40	96-302
			300	108-298

ously mentioned, either perpendicular to pseudocubic axes, or perpendicular to orthorhombic axes. The recorded Raman spectra exhibit 18 lines of the 24 lines expected by group-theory calculations. An assignment was suggested considering the Raman spectra in parallel and crossed configurations observed at 40 and 300 K for the two oriented samples. It can be noticed that the $7A_g$ modes are identified but only $4B_{1g}$ were detected among the five predicted, likewise $5B_{2g}$ modes are evidenced compared to the $7B_{2g}$ expected, and only $2B_{3g}$ modes were observed among the $5B_{3g}$ calculated. All missing lines could not be detected in spite of repeated efforts: high-power laser, spectra accumulation duration. Table IV summarizes the assignment proposed at 40 and 300 K, and Fig. 4 exhibits Raman spectra in the different orthorhombic configurations at low temperature. However, it

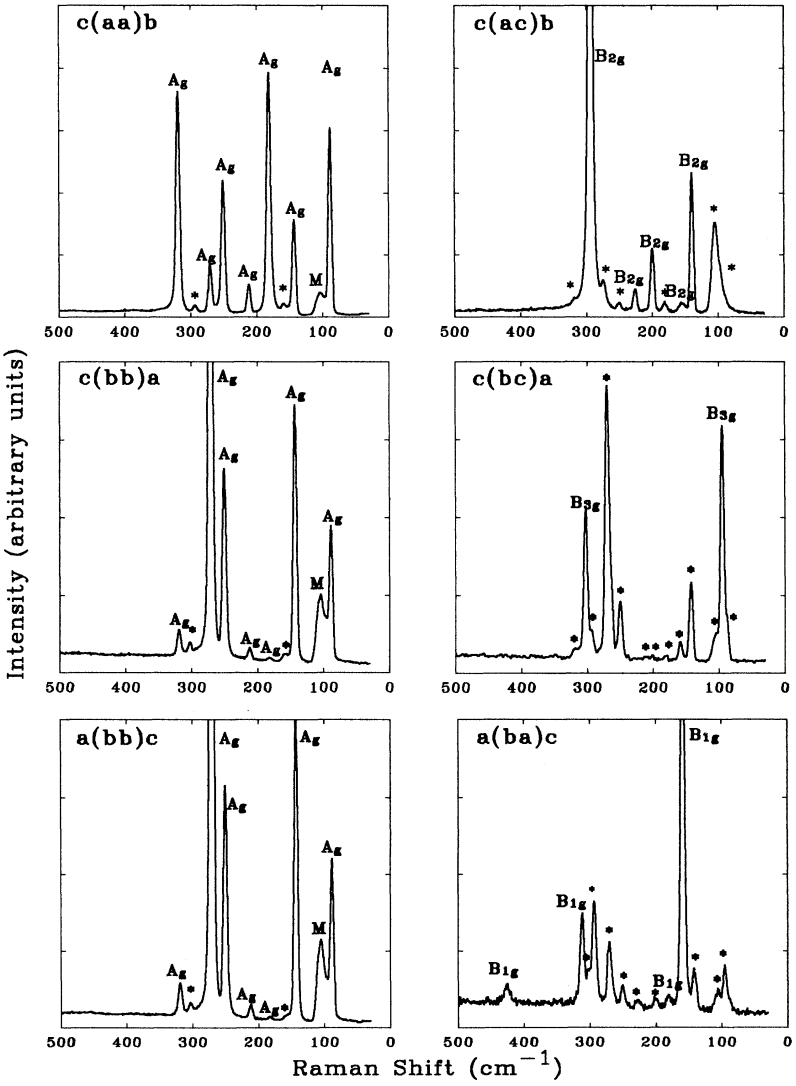

FIG. 4. Raman spectra obtained in the six different orthorhombic configurations at 40 K. Asterisks indicate polarization leaks.

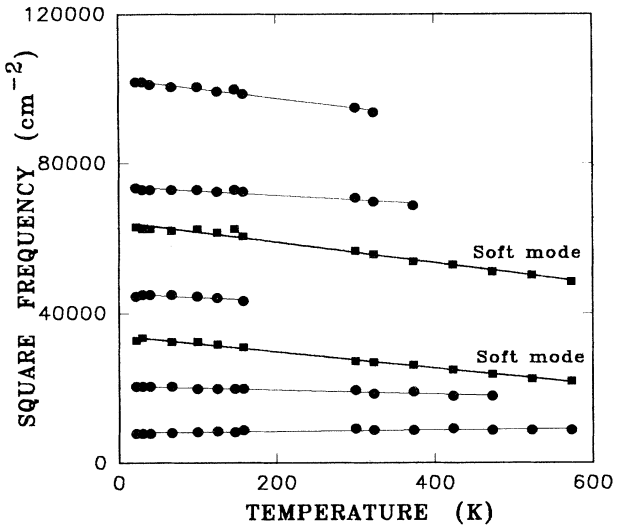

FIG. 5. Square frequencies of A_g orthorhombic lines as a function of temperature.

is important to notice that, because of the minor proportions of domains in the crystals (7% of $[100]_o$ domains in the $[001]_o$ direction or 1% of $[001]_o$ domains in the $[100]_o$ direction), leaks of unexpected modes have been observed in the same proportions on polarized spectra.

High-temperature measurements were also attempted by Raman scattering; unfortunately, above 573 K, the samples were damaged and oxidation on the surface made it impossible to carry on experiments up to the transition temperature. As evidenced in Fig. 5 a softening of all $7\,A_g$ observed Raman lines can be observed up to 573 K. Among these seven lines, five lines exhibit a weak softening corresponding to the usual behavior of Raman lines versus temperature while the two A_g modes, respectively, located at 183 and 250 cm^{-1} at 40 K, exhibit more important broadening and decreasing of frequency with temperature increasing (see Fig. 5). Then these two last modes can be attributed to soft modes of the orthorhombic phase responsible for the transition. As usual, this behavior can be fairly well described by a Landau law:

$$\omega^2 = a(T - T_0)\ ,$$

where $T_0 \sim 1500$ K, which corresponds, as usually observed, to a higher temperature than the real transition temperature $T_c = 965$ K. This result will be discussed later. Moreover this study allows us to identify which mode is responsible for the transition in the orthorhombic phase and then it can be deduced from compatibility diagrams that these modes correspond to the R'_{15} and M_2 zone-boundary modes in the cubic phase. This information will be essential for lattice-dynamics calculations. Evolution of B_{1g}, B_{2g}, or B_{3g} orthorhombic modes could not be followed versus temperature because of their too weak intensities.

We report also an observation of a two-magnon Raman mode due to the antiferromagnetic character of $NaMnF_3$ below the Néel temperature. This two-magnon mode can

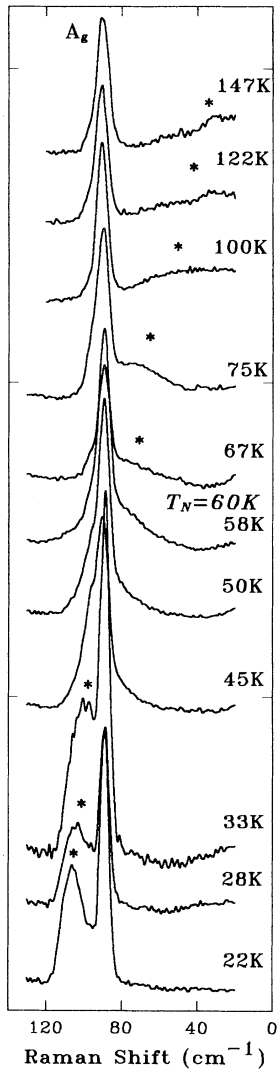

FIG. 6. Temperature dependence of the two-magnon Raman mode in $NaMnF_3$. Asterisks indicate the location of the two-magnon mode.

be recognized by its shape and its temperature dependence. As shown in Fig. 6 the two-magnon spectrum broadens and shifts from 105 cm^{-1} at 22 K to 75 cm^{-1} at 75 K. Some scattering is still observable at 150 K although precise location of the peak is difficult. These experimental data are consistent with previous studies like neutron diffraction,[17] antiferromagnetic resonance,[18] giving $T_N = 60$ K. This result can be also compared to the same kind of magnetic transitions occurring in $KMnF_3$ at $T_N = 88$ K (Ref. 19) and $RbMnF_3$ at $T_N = 82.5$ K,[20] especially the persistence of a two-magnon Raman signal was often previously observed in other compounds of which the crystal structure is close to the $NaMnF_3$ one.

LATTICE DYNAMICS

Knowledge of the phonon spectrum in the cubic phase of $NaMnF_3$ is needed in order to get information on the

origin of the transitions. In the present case using a rigid ion model, the phonon spectrum depends on a small set of parameters which can be adjusted from Raman data alone as measured in the orthorhombic phase since most of them are not strongly dependent on this structure. In the harmonic approximation, the potential energy is defined by a sum of second-order terms. Moreover, neglecting the electronic polarizability, it is convenient to distinguish the long-range electrostatic forces from the short-range interaction between nearest-neighbor ions. The long-range part of the dynamical matrix is calculated with the help of a standard program and depends only on the atomic positions and on the effective ionic charges Z_i^*. The short-range dynamical matrix is determined for the case of axially symmetric forces. Thus it involves two parameters A_i, B_i, which correspond to the second derivative of the short-range potential function V_i, parallel and perpendicular to the line joining the interacting ions. These undimensionless coefficients are classically defined in the CGS system by

$$A_i = \left[\frac{2v}{e^2}\right]\left[\frac{\partial^2 V_i}{\partial r_{i\parallel}^2}\right], \quad B_i = \left[\frac{2v}{e^2}\right]\left[\frac{\partial^2 V_i}{\partial r_{i\perp}^2}\right],$$

where e is the elementary charge ($e = 4.803 \times 10^{-10}$ CGS units) and v the volume of the cubic unit cell.

In the more appropriate MKS system, we use the following relations:

$$A_i = \left[\frac{8\pi\varepsilon_0 v}{e^2}\right]\left[\frac{\partial^2 V_i}{\partial r_{i\parallel}^2}\right], \quad B_i = \left[\frac{8\pi\varepsilon_0 v}{e^2}\right]\left[\frac{\partial^2 V_i}{\partial r_{i\perp}^2}\right],$$

where $e = 1.602 \times 10^{-19}$ C.

In this system we define the A_i' and B_i' parameters, expressed in N m^{-1}, through the relations:

$$A_i' = \left[\frac{e^2}{8\pi\varepsilon_0 v}\right] \times A_i = \left[\frac{\partial^2 V_i}{\partial r_{i\parallel}^2}\right],$$

$$B_i' = \left[\frac{e^2}{8\pi\varepsilon_0 v}\right] \times B_i = \left[\frac{\partial^2 V_i}{\partial r_{i\perp}^2}\right].$$

Then, in case of the fluoroperovskite $NaMnF_3$, the adjustable parameters of the lattice-dynamics model are labeled $A_1, B_1, A_2, B_2, A_3, B_3$ and $Z_{Na}^*, Z_{Mn}^*, Z_F^*$. The subscript 1 corresponds to the Na-F interaction, while the subscript 2 is for the Mn-F interaction and 3 for the F-F interaction. Z_{Na}^*, Z_{Mn}^*, and Z_F^* indicate the effective ionic charges which are linked by the electric neutrality equation: $Z_{Na}^* + Z_{Mn}^* + 3Z_F^* = 0$.

Neglecting Van der Waals interactions, the short-range potential energy between a pair of ions interacting through central forces is assumed in this model to be expressed with the Born-Mayer form:

$$V_i = \lambda_i \exp\left[\frac{-r_i}{\rho_i}\right],$$

where r_i is the interionic distance and λ_i, ρ_i characteristic constants of the pair of ions. So the parameters A_i, B_i previously defined can be expressed versus λ_i and ρ_i by

$$A_i' = \frac{\lambda_i}{\rho_i^2}\exp\left[\frac{-r_i}{\rho_i}\right], \quad B_i' = -\frac{\lambda_i}{r_i\rho_i}\exp\left[\frac{-r_i}{\rho_i}\right]$$

and then

$$\frac{A_i'}{B_i'} = \frac{A_i}{B_i} = -\frac{r_i}{\rho_i}.$$

First a set of parameters was estimated to perform calculations. Considering the influence of the tilting of the MnF_6 octahedra (8.5°: Ratuszna *et al.*[14]) on the fluorine-fluorine distance in the orthorhombic phase, the average F-F distance was assumed to be about 2.9 Å. Moreover according to Salaün and Rousseau,[21] who previously established a linear law between $\ln(A_3/V)$ versus F-F interionic distance for AMF_3 perovskite crystals, the ρ value for F-F interaction can be fixed to 0.582 Å. This estimated ρ value can be anyway applied successfully in other various derived structures like MF_3 and AMF_4 compounds for which dynamical data were available.[22,23] Then in case of $NaMnF_3$ according to the F-F distance we deduce that $A_3/B_3 \approx -5$. Concerning the manganese-fluorine interaction, Becher *et al.*[24] and Watson *et al.*[25] previously determined, in $KMnF_3$, that $\rho \approx 0.275$ Å. Transposing this value to $NaMnF_3$ [with d(Mn-F) = 2.1 Å], it could be concluded that $A_2/B_2 \approx -7.64$. For the sodium-fluorine interaction it was roughly estimated, like in alkali halides,[26,27] that $A_1/B_1 \approx -10$. The attribution of an ionic effective charge Z_i^* to the ions of the structure is a phenomenological manner to take the electronic polarizability into account in a rigid ion model. For most of fluoroperovskites the ratio Z_i^*/Z_i lies between 0.73 and 0.82; following Salaün and Rousseau,[21] we chose to impose Z_i^*/Z_i to the mean value 0.77. Then we fixed $Z_{Na} = 0.77$, $Z_{Mn} = 1.4$, and $Z_F = -0.77$.

From all these assumptions, only three parameters A_1, A_2, and A_3 were unknown and then were crudely taken to "usual" values as a first set of parameters in the fitting procedure. All these parameters were introduced in a standard program calculating eigenfrequencies and eigenmodes in the cubic phase at all points of the first cubic Brillouin zone. With the help of compatibility relations between orthorhombic and cubic symmetry, and a direct fit of the Raman modes which are temperature independent, a final set of parameters was deduced (Table V).

TABLE V. Parameters of the rigid ion model in the cubic phase of $NaMnF_3$ estimated from temperature-independent Raman frequencies of the orthorhombic phase. Interaction force constants are given either in conventional units (c.u.; CGS system) or in N/m (international system). 1,2,3 subscripts indicate, respectively, Na-F, Mn-F, F-F interactions. $Z_{Na}^* = 0.77$, $Z_{Mn}^* = 1.54$, $Z_F^* = -0.77$; $A_1/B_1 = -10$, $A_2/B_2 = -7.64$, $A_3/B_3 = -5$.

	A_1	B_1	A_2	B_2	A_3	B_3
c.u.	5.0	−0.50	62.0	−8.08	5.36	−1.09
N/m	9.08	−0.908	112.59	−14.67	9.73	−1.98

TABLE VI. Calculated zone-boundary frequencies in the cubic phase of $NaMnF_3$ compared to corresponding experimental Raman frequencies of the orthorhombic phase. (1) Cubic zone-boundary modes corresponding to active Raman modes in the orthorhombic phase (given in Koster labeling; Mn^{2+} origin). (2) Orthorhombic raman active modes connected to cubic mode with compatibility diagram. (3) Experimental Raman frequencies at 40 K; nonobserved lines are indicated by a slash. (4) Average of the experimental Raman frequencies coming from degenerated cubic zone-boundary modes. (5) Calculated cubic frequencies by the rigid ion model with parameters of Table V. (6) Absolute difference between calculated and experimental frequencies; a slash indicates cases where calculations are impossible or without signification. (7) Relative difference between calculated and experimental frequencies.

(1) Cubic modes	(2) Orthorhom. modes	(3) Exp. (cm^{-1})	(4) Exp. Avera. (cm^{-1})	(5) Calc. (cm^{-1})	(6) $\Delta\omega$ (cm^{-1})	(7) $\Delta\omega/\omega$ (%)
R'_{15}	A_g	183	183	−110.6	/	/
	B_{1g}	/				
	B_{2g}	/				
R'_{25}	A_g	143	131.3	137.6	6.3	4.58
	B_{2g}	155				
	B_{3g}	96				
R'_{25}	A_g	270	248	296.0	48	16.2
	B_{2g}	226				
	B_{3g}	/				
R_{12}	B_{1g}	312	307	307.4	0.4	0.13
	B_{3g}	302				
R_1	B_{3g}	/	/	490.4	/	/
M_2	A_g	250	250	−110.0	/	/
M_5	B_{1g}	160	160	161.7	1.7	1.05
	B_{3g}	/				
M_4	B_{2g}	293	293	308.6	15.6	5.05
M_3	A_g	319	319	307.6	11.4	3.71
M_1	B_{2g}	/	/	449.4	/	/
X_5	A_g	88	114.5	117.0	2.5	2.14
	B_{2g}	140				
X_1	B_{1g}	182	182	178.8	3.2	1.79
X_5	A_g	212	206.5	164.8	41.7	25.3
	B_{2g}	201				
X_1	B_{1g}	426	426	408.1	17.9	4.39

The value deduced from our fit for the F-F interaction force constant is in good agreement with the one suggested by Salaün and Rousseau[21] for this fluoroperovskite.

Table VI shows results of the last fit comparing experimental Raman frequencies of the orthorhombic room-temperature phase with the corresponding eigenfrequencies in the pseudocubic phase calculated by the rigid ion model at the R_c, M_c, and X_c zone boundary points.

A fairly good agreement is generally observed between theoretical and experimental data, except for octahedra rotation modes responsible for the transition (R'_{15} and M_2), which are soft modes characteristic of the displacive character of that kind of transition. This discrepancy is not surprising because the frequencies of these unstable modes are widely affected by very small changes in the model's parameters. After determining the parameters of the cubic phase from the low-temperature orthorhombic phase data, the calculated frequencies revealed the instability of the cubic phase at this temperature in giving some negative eigenvalues of the dynamical matrix. These negative values of square frequencies ω^2 correspond to imaginary frequencies $i\omega$ which are noted, by continuity $-\omega$ in our dispersion curves.

Moreover, in Table VI, when orthorhombic modes give rise to degenerate cubic modes, calculated frequencies are compare to the average of the corresponding experimental frequencies. It can be also noticed that calculated frequencies in the cubic phase of X_5 and R'_{25} modes exhibit a fairly large discrepancy compared to the experimental one. These modes correspond to the most important splitting amplitude in the orthorhombic symmetry. Moreover calculations of the eigenvectors with the model show that the X_5 and R'_{25} modes of the cubic phase induce ionic displacement of Na^+ along $[101]_c$; now, the structural work of Ratuszna, Majewska, and Lis[15] evidences the displacements of Na^+ cation along this direction, which confirms the fairly large discrepancy observed for these modes between calculated and experimental frequencies. Furthermore knowing that the Na-F distances are displayed on a wide range from 2.29 to 2.67 Å in the low-symmetry phase, the Na-F interionic constant can be very affected. The adopted value corresponds only to an average Na-F distance and then cannot account for the real interaction between ions.

TABLE VII. Elastic constants of $NaMnF_3$ at room temperature measured by Brillouin scattering in a pseudocubic configuration. Experimental data are compared to elastic constants calculated with the rigid ion model and to experimental ones of $KMnF_3$ and $RbMnF_3$. Measurements are performed in a pseudocubic configuration. Average refraction index is $n = 1.4316$ (Pulfrich refractometer experiment).

	a_{cub} (Å)	C_{11} (GPa)	C_{12} (GPa)	C_{44} (GPa)	References
$NaMnF_3$ expt.	3.99	108.2(1.8)	44(20)	26.7(0.5)	This work
$NaMnF_3$ calc.		114.2	48.93	27.74	This work
$KMnF_3$ expt.	4.19	115(1)	39.5(1)	27.4(1)	25
$RbMnF_3$ expt.	4.239	117.4(0.2)	42.1(0.4)	31.9(0.1)	26

Furthermore, calculated frequencies were also compared to active infrared spectroscopic frequencies recorded by Lane *et al.*[28] A fairly good agreement seems to be evidenced for most frequencies, however we have to be prudent and a significative comparative table cannot be given, since Lane *et al.* were unable to assign infrared spectra to irreducible representations of the D_{2h} point group.

Following Rousseau *et al.*[29] and Cowley,[30] the elastic constants can be exactly expressed in terms of the nine former parameters of the model. Indeed, every ion is located at a center of symmetry and the polarizabilities do not affect the elastic constants. In order to confirm calculations, the predicted elastic constants were compared to those measured at room temperature by Brillouin scattering, assuming a pseudocubic approximation. Table VII exhibits experimental and theoretical constants. As previously mentioned, the orthorhombic distortion weakly affects C_{11} and C_{44}, whereas C_{12} is significantly more sensitive. However, a good agreement between the mean experimental and theoretical determinations is observed which validates the chosen values of our lattice-dynamics parameters. Reported data are also close to those previously measured in $KMnF_3$ (Ref. 31) and $RbMnF_3$ (Ref. 32).

An estimation of the interaction force constants makes it possible to calculate the whole phonon spectrum, as shown in Fig. 7, in the cubic symmetry. One important characteristic of this phonon spectrum is the existence of a low-frequency R'_{15}-M_2 quasiflat line, corresponding to rotations of octahedra around fourfold cubic axes. Existence of such a flat phonon branch suggests, as previously proposed by Rousseau[33] and Bulou *et al.*,[34] that the mechanism of the SPT can be connected to condensation of the whole phonon branch and is due to the natural competition between R'_{15} and M_2 modes.

A knowledge of the phonon spectrum makes it possible to predict some additional dynamical properties of $NaMnF_3$ such as the one-phonon density of states. This has been calculated using a mesh of 10^6 q vectors in the $\frac{1}{16}$th volume of the first Brillouin zone with a frequency interval of 1 cm^{-1}. The result is plotted in Fig. 8. Two important gaps close to 300 and 410 cm^{-1} are observed. The cutoff frequency is located at 490 cm^{-1}, which is a low value compared to that in other fluoroperovskites.

CONCLUSION

For the first time in fluoroperovskites AMF_3, to our knowledge, a Raman scattering study of the low-

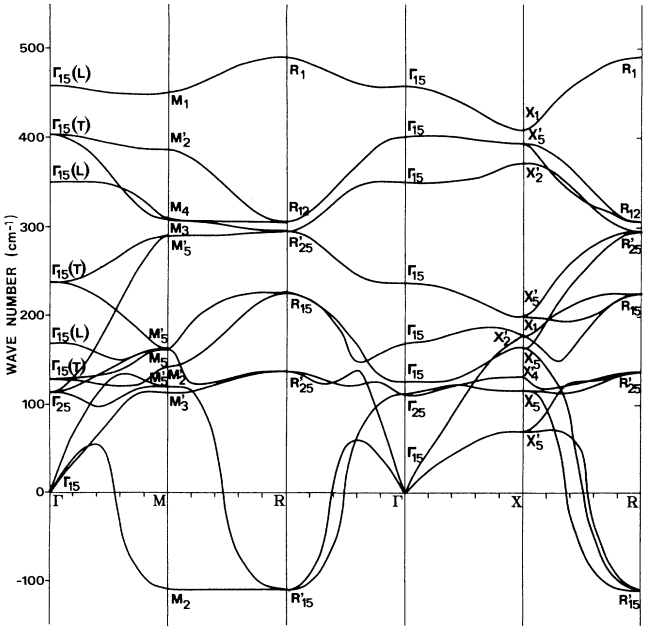

FIG. 7. Calculated phonon spectrum of $NaMnF_3$ in the cubic symmetry.

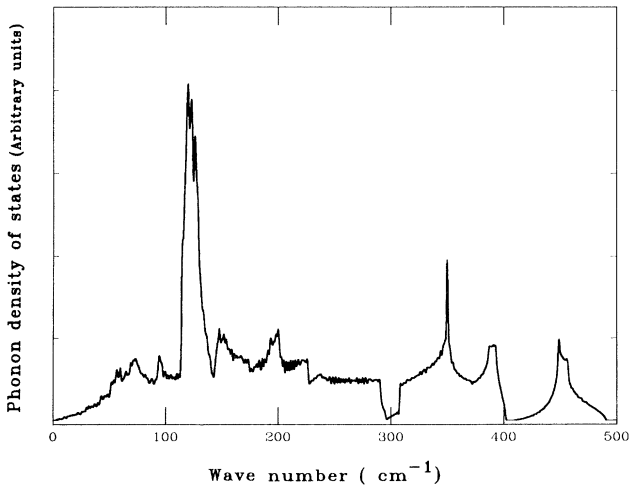

FIG. 8. Calculated one-phonon density of states of $NaMnF_3$ in the cubic symmetry.

temperature phase was performed and fully interpreted in the case of a monodomain crystal of $NaMnF_3$. All observed lines were attributed on the basis of a group-theory analysis. This Raman work will be very useful to explain Raman data in other isostructural materials which are usually polydomains in the orthorhombic symmetry and may be able to contribute important information concerning the mechanism of the SPT.

The lattice dynamics of the cubic phase of $NaMnF_3$ has been analyzed in terms of a rigid ion model. Indeed Raman data appear to be sufficient to predict the whole phonon spectrum and calculate the one-phonon density of states of this material, with help of compatibility diagrams between cubic and orthorhombic symmetries.

A complete agreement is obtained between calculated and measured Raman frequencies which are temperature independent. Theoretical elastic constants deduced from the model are also very close to those measured by Brillouin scattering. The calculations show the existence of a quasiflat line phonon branch R'_{15}-M_2, the two extremities of which are responsible for the transition. This flat branch, usually observed in fluoroperovskites that exhibit SPT, corresponds to a natural competition between "ferro" and "antiferro" coupling of adjacent octahedra planes perpendicular to the $[010]_c$ rotation axis. Raman spectra at high temperature evidence the existence of two soft modes in the orthorhombic phase. According to the compatibility diagram, these two modes give rise to R'_{15} and M_2 soft modes of the cubic phase. Moreover, the observed difference between the real transition temperature ($T_c = 965$ K) and the temperature suggested by extrapolation of a Landau behavior of square frequencies of orthorhombic A_g soft modes ($T_o \approx 1500$ K) seems to indicate that the mechanism of this transition can be considered as of first-order character. Furthermore, the observation of the quasimonodomain character of this perovskite should indicate that no intermediate tetragonal phase exists. It can then be deduced that the condensations of R'_{15} and M_2 modes of the cubic Brillouin zone are probably simultaneous.

We are now planning an extensive study in $NaMgF_3$ and $NaZnF_3$, which exhibit the same kind of SPT, in order to shed light on this aspect of the transition mechanism in fluoroperovskites.

ACKNOWLEDGMENTS

This work was performed and financially supported in the framework of an integrated action (ATP S04) between the French Ambassy in Poland, the French Foreign Office in Paris, and the Institute of Physics of the University of Silesia in Katowice (Poland). Especially, we are very much indebted to D. Le Masne and his staff for their contribution in the realization of this scientific program. We would like to thank G. Niesseron for his help with crystal growth, and special thanks go to A. Gibaud and S. Salaün for many valuable and interesting discussions. The help of A. Bulou in group-theory calculations and the critical reading of J. Toulouse (Lehigh University–Bethlehem–USA) were invaluable, thus we wish also to thank them for their efficient contribution.

[1]J. W. Flocken, R. A. Guenther, J. R. Hardy, and L. L. Boyer, Phys. Rev. Lett. **56**, 1738 (1986).
[2]U. J. Cox, A. Gibaud, and R. A. Cowley, Phys. Rev. Lett. **61**, 982 (1988).
[3]M. Hidaka, Z. Y. Zhou, and S. Yamashita, Phase Trans. **20**, 83 (1990).
[4]J. Fayos and J. Tornero, Ferroelectrics Lett. **16**, 43 (1993).
[5]F. Koussinssa and M. Diot, Thermochim. Acta **216**, 87 (1993).
[6]A. Ratuszna, J. Phys. Condens. Matter **5**, 841 (1993).
[7]Y. Zhao *et al.*, Phys. Earth Planet. Inter. **76**, 1 (1993).
[8]A. M. Debaud-Minorel and J. Y. Buzaré, J. Phys. Condens. Matter **6**, 2189 (1994).
[9]A. M. Glazer, Acta Crystallogr. A **31**, 756 (1975).
[10]F. A. Kasan-Ogly and V. E. Naish, Acta Crystallogr. B **42**, 325 (1986).
[11]D. Skrzypek, P. Jakubowski, and A. Ratuszna, J. Cryst. Growth **48**, 475 (1980).
[12]J. Nouet (private communication).
[13]A. Bulou, J. Nouet, A. W. Hewat, and F. J. Schafer, Ferroelectrics **25**, 375 (1980).
[14]A. Katrusiak and A. Ratuszna, Solid State Commun. **84**, 435 (1992).
[15]A. Ratuszna, K. Majewska, and T. Lis, Acta Crystallogr. C **45**, 548 (1989).
[16]D. L. Rousseau, R. P. Bauman, and S. P. S. Porto, J. Raman Spectrosc. **10**, 253 (1981).
[17]S. J. Pickart, H. A. Alperin, and R. Nathans, J. Phys. **25**, 565 (1964).
[18]D. T. Teaney, J. S. Blackburn, and R. W. H. Stevenson, J. Am. Phys. Soc. **7**, 201 (1962).
[19]G. Shirane, V. J. Minkiewicz, and A. Linz, Solid State Commun. **8**, 1941 (1970).
[20]P. A. Fleury, Phys. Rev. Lett. **21**, 151 (1968).
[21]S. Salaün and M. Rousseau, Phys. Rev. B (to be published).
[22]P. Daniel *et al.*, Phys. Rev. B **42**, 10 545 (1990).
[23]A. Bulou, M. Rousseau, J. Nouet, and B. Hennion, J. Phys. Condens. Matter **1**, 4553 (1989).
[24]R. R. Becher, M. J. Sangster, and D. Strauch, J. Phys. Condens. Matter **1**, 7801 (1989).
[25]G. W. Watson, S. C. Parker, and A. Wall, J. Phys. Condens. Matter **4**, 2097 (1992).
[26]K. V. Namjoshi, S. S. Mitra, and J. F. Vetelino, Phys. Rev. B **3**, 4398 (1970).
[27]M. P. Tosi, *Solid State Physics* (Academic, New York, 1964), Vol. 16.
[28]A. P. Lane *et al.*, J. Chem. Soc. A 94 (1971).
[29]M. Rousseau, J. Nouet, and A. Zarembovitch, J. Phys. Chem. **35**, 921 (1974).
[30]R. A. Cowley, Phys. Rev. **134**, 981 (1964).
[31]K. S. Aleksandrov *et al.*, Phys. Status Solidi **18K**, 17 (1966).
[32]R. L. Melcher and D. F. Bolef, Phys. Rev. **178**, 864 (1969).
[33]M. Rousseau, J. Phys. Lett. **40**, 439 (1979).
[34]A. Bulou, M. Rousseau, and J. Nouet, Ferroelectrics **104**, 373 (1990).